



THE UNIVERSITY *of* EDINBURGH

## Edinburgh Research Explorer

### Tidal Range Resource of Australia

**Citation for published version:**

Neill, SP, Hemmer, M, Robins, PE, Griffiths, A, Furnish, A & Angeloudis, A 2021, 'Tidal Range Resource of Australia', *Renewable Energy*, vol. 170, pp. 683-692. <https://doi.org/10.1016/j.renene.2021.02.035>

**Digital Object Identifier (DOI):**

[10.1016/j.renene.2021.02.035](https://doi.org/10.1016/j.renene.2021.02.035)

**Link:**

[Link to publication record in Edinburgh Research Explorer](#)

**Document Version:**

Publisher's PDF, also known as Version of record

**Published In:**

Renewable Energy

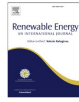
**General rights**

Copyright for the publications made accessible via the Edinburgh Research Explorer is retained by the author(s) and / or other copyright owners and it is a condition of accessing these publications that users recognise and abide by the legal requirements associated with these rights.

**Take down policy**

The University of Edinburgh has made every reasonable effort to ensure that Edinburgh Research Explorer content complies with UK legislation. If you believe that the public display of this file breaches copyright please contact [openaccess@ed.ac.uk](mailto:openaccess@ed.ac.uk) providing details, and we will remove access to the work immediately and investigate your claim.





## Tidal range resource of Australia

Simon P. Neill<sup>a,\*</sup>, Mark Hemmer<sup>b</sup>, Peter E. Robins<sup>a</sup>, Alana Griffiths<sup>a</sup>, Aaron Furnish<sup>a</sup>, Athanasios Angeloudis<sup>c</sup><sup>a</sup> School of Ocean Sciences, Bangor University, Marine Centre Wales, Menai Bridge, UK<sup>b</sup> CSIRO Oceans and Atmosphere, Hobart, Australia<sup>c</sup> School of Engineering, Institute for Infrastructure & Environment, University of Edinburgh, Edinburgh, UK

## ARTICLE INFO

Article history:  
Received 25 November 2020  
Received in revised form  
3 February 2021  
Accepted 6 February 2021  
Available online 9 February 2021

Keywords:  
Tidal range power  
Tidal lagoons  
Tidal barrage  
OD modelling  
TPX09  
Australia

## ABSTRACT

In some shelf sea regions of the world, the tidal range is sufficient to convert the potential energy of the tides into electricity via tidal range power plants. As an island continent, Australia is one such region – a previous study estimated that Australia hosts up to 30% of the world's resource. Here, we make use of a gridded tidal dataset (TPX09) to characterize the tidal range resource of Australia. We examine the theoretical resource, and we also investigate the technical resource through OD modelling with tidal range power plant operation. We find that the tidal range resource of Australia is 2004 TWh/yr, or about 22% of the global resource. This exceeds Australia's total energy consumption for 2018/2019 (1721 TWh/yr), suggesting tidal range energy has the potential to make a substantial contribution to Australia's electricity generation (265 TWh/yr in 2018/2019). Due to local resonance, the resource is concentrated in the sparsely populated Kimberley region of Western Australia. However, the tidal range resource in this region presents a renewable energy export opportunity, connecting to markets in southeast Asia. Combining the electricity from two complementary sites, with some degree of optimization tidal range schemes in this region can produce electricity for 45% of the year.

© 2021 The Author(s). Published by Elsevier Ltd. This is an open access article under the CC BY license (<http://creativecommons.org/licenses/by/4.0/>).

## 1. Introduction

Among the various types of ocean renewable energy conversion, including wave energy and offshore wind, one form has the major advantage of predictability – tidal energy. Although most research and commercial developments are currently based on exploiting the kinetic energy of the tides via in stream tidal energy converters, there is presently more globally installed tidal range capacity (around 500 MW, compared to around 10 MW of tidal stream), and indeed both forms (tidal stream and tidal range) have approximately equal global potential [1]. Among potential sites, Australia has the largest concentration of tidal range resource in the world, previously estimated as around 30% of the global resource [2].

Australia's electricity sector is the country's largest CO<sub>2</sub> emitting industry, responsible for 32% of the country's overall greenhouse gas emissions [3]. In 2019, 24% of Australia's power generation came from renewable sources [4]. Energy scenarios have already been simulated in which 100% of the demand of the Australian

National Electricity Market could be met using renewable sources; however these scenarios focussed on technologies that are already commercially available such as existing hydro and biofuelled turbines, solar, and wind [5]. Further, such a change in the generation mix would need to be supported by an expansion of the transmission grid, including strategically placed interconnectors and the development of renewable energy zones, coupled with energy storage [6]. Australia has some of the world's strongest semi-diurnal and diurnal tides, with the Kimberley region of north-western Australia hosting some of the largest tidal ranges in the world, and almost all of Australia's exploitable tidal range resource [7]. Australia's tidal stream resources are distributed nationally, although sites proximal to identified demand near Darwin in the Northern Territory and Banks Strait, in south-eastern Bass Strait near Tasmania have received focussed attention [8].

Doctor's Creek, located in the southern part of King Sound in Western Australia, has been the subject of various proposals for tidal range energy plants since the 1960s [9]. In 1999 a proposal investigated the feasibility of a 48 MW two-basin tidal barrage scheme at Doctor's Creek, which, at that time, would have made it the second largest tidal power plant in the world, with the two-basin design minimizing variability in the power output [10]. In

\* Corresponding author.  
E-mail address: [s.p.neill@bangor.ac.uk](mailto:s.p.neill@bangor.ac.uk) (S.P. Neill).

2013, this project received EPA (Environmental Protection Authority) approval (now lapsed) but was unable to attract funding.

Tidal range power plants are a mature technology, with a history extending back to the development of La Rance tidal barrage, which has been operating since 1966 [11]. A tidal barrage consists of an embankment (the major capital cost of the power plant) that impounds water upstream. In a fairly conventional operating mode, known as *ebb-generation*, sluice gates in the embankment remain open during the flood phase of the tidal cycle, and the water level upstream of the barrage increases at the same rate as the water level outside of the impoundment. At high water, the sluice gates are closed, and the water level outside of the impoundment naturally ebbs, whereas the water level inside the impoundment remains at “high water” (a period known as holding). Once sufficient head is generated, the water inside the impoundment is directed through turbines in the embankment to turn a generator, producing electricity. When the head is insufficient to economically drive the turbines, the sluice gates are closed. During the subsequent flood phase of the tide, the sluice gates are again open and the process repeats. All existing tidal range schemes throughout the world are barrages [2]. However, a more recent concept of the tidal lagoon (where an estuary or body of water is only partially impounded) is gaining popularity, particularly as the construction costs and environmental impacts of a lagoon are considerably less than that of a barrage [12]. This additionally opens up regions of high tidal range that were previously considered unfeasible due to lack of an estuary or seaway to construct a barrage.

In this article we make use of the  $1/30 \times 1/30^\circ$  TPX09-v2 global dataset to examine the tidal range resource of Australia, from both theoretical and technical perspectives. After introducing the hydrography of the study region (Section 2), the methods used to calculate the theoretical and technical resource are detailed in Section 3. The results are presented in Section 4 for the global and regional resource, followed by examination of the technical resource of two sites in Western Australia. Finally, the practical constraints and opportunities for tidal power schemes in Australia are discussed (Section 5), including the potential for reduced power variability by aggregating the output from multiple sites that are complementary in phase.

### 1.1. Hydrography and electrical grid system of Australia

As an island continent, Australia is entirely surrounded by seas and oceans, including the Indian Ocean to the west, the South Pacific Ocean to the east, and the Southern Ocean to the south (Fig. 1). The continental shelf of Australia is relatively narrow to the south and east, and wider across the north. As the shelf seas are relatively wide in the north and west, this leads to tidal resonance (particularly in the Timor Sea), and hence amplified tidal ranges in these areas [13]. The tides are generally semi-diurnal, but diurnal tides dominate to the southwest and in the Gulf of Carpentaria in the north (Fig. 2). In many regions of Australian coastal waters, the tides are mixed, i.e. predominantly semi-diurnal but with a significant diurnal component.

Co-tidal charts of the five largest tidal constituents around Australia (M2, S2, N2, K1, O1) further demonstrate the dominance of the semi-diurnal constituents, and show that the tidal range is largest in the northwest due to tidal resonance (Fig. 3). Although the co-tidal lines show an amphidromic point near Perth in the southwest (for example in the M2 and S2 constituents), there is a distinct lack of co-tidal lines in the northwest, particularly in the Kimberley region – indicative of a standing wave system [1].

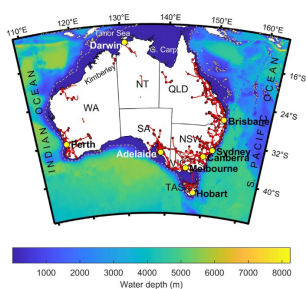


Fig. 1. Bathymetry (metres relative to MSL) around Australia, with major electricity substations ( $> 110$  V) shown as red dots, and transmission lines also in red. Australian states: NSW – New South Wales, QLD – Queensland, SA – South Australia, TAS – Tasmania, VIC – Victoria, WA – Western Australia, NT – Northern Territory, G. Carp. is the Gulf of Carpentaria. The dashed yellow line is the 200 m depth contour. Bathymetry data from TPX09, and substation/transmission line data from Geoscience Australia.

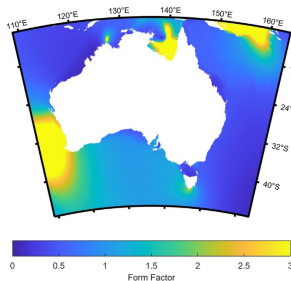


Fig. 2. Form Factor ( $F$ ) for Australian waters, showing the ratio between diurnal and semi-diurnal tides ( $F = (H_{K1} + H_{O1}) / (H_{M2} + H_{S2})$ ). For interpretation,  $0 < F < 0.25$  is semi-diurnal,  $0.25 < F < 1.5$  is mixed (mainly semi-diurnal),  $1.5 < F < 3$  is mixed (mainly diurnal), and  $F > 3$  is diurnal.

Therefore, in regions of high tidal range, there is unlikely to be sufficient phase diversity to stagger tidal range power plants, which would reduce variability in the aggregated power signal [14,15]. In the Kimberley region, the semi-diurnal constituents reach their maximum values of around 3 m (M2) and 2 m (S2). In contrast, the diurnal constituents reach values of around 0.6 m (K1) and 0.3 m (O1) just to the east of Kimberley – in the Joseph Bonaparte Gulf.

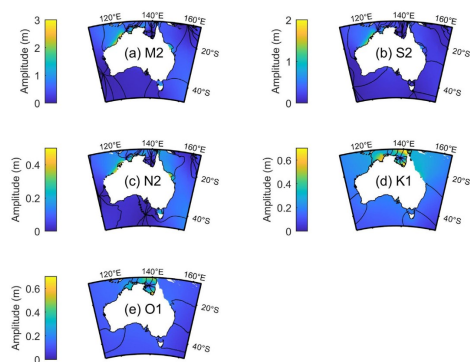


Fig. 3. Co-tidal charts for the five dominant diurnal and semi-diurnal tidal constituents around Australia – (a) M2, (b) S2, (c) N2, (d) K1, and (e) O1. Colour scale is amplitude, and black contours are co-tidal lines, connecting regions that are equal in tidal phase. Data from TPX09-v2.

Therefore, in regions of high tidal range, the tides are strongly semi-diurnal (Form Factor,  $F = 0.1$ ) in the Kimberley region, but mixed (mainly semi-diurnal,  $F = 0.3$ ) in the Joseph Bonaparte Gulf.

Australia is one of the most urbanized countries in the world, with over 90% of the population living within just 0.22% of its land area. 85% of Australia's population live within 50 km of the coast. The distribution of this population is predominantly in the eastern cities of Sydney (NSW), Melbourne (VIC), and Brisbane (QLD). These States, along with SA, Tasmania and ACT share a common electricity grid – the National Electricity Market (NEM). Perth, WA's capital city, is located in the southwest of the continent, and is served by an independent electricity grid – the South-West Interconnected System. Smaller grids are located in the northwest of WA (the North-West Interconnected System) and in Darwin (the Darwin-Katherine Electricity Network). Vast unpopulated areas separate these grid systems – Australia's mean population density is one of the lowest in the world ( $3.3/\text{km}^2$ ).

Because Australia's electricity system is fragmented, and there is a lack of grid connectivity between states, it is not possible for power generated on one side of the country to be transmitted to the other. Sydney, Melbourne and Brisbane, Australia's three most populous cities, are all in the east or south east of the country and are connected to the NEM electricity grid. The Kimberley region of Western Australia is remote from the electrical grid system. The existing infrastructure would not allow for electricity generated in the north-west of the country, i.e. from tidal range schemes, to reach the south-east where the majority of demand occurs. The Kimberley region itself (the region with the highest tidal ranges) has no major cities; the closest are Perth 1800 km to the south and Darwin 400 km to the east, covered respectively by the SWIS and the Darwin-Katherine Electricity Network. For the Kimberley region, in addition to local consumption, this could represent a strategic export market for renewable electricity [16–18].

## 2. Methods

In this section we describe the TPX09-v2 dataset, and our methods for calculating the theoretical and technical tidal range resource.

### 2.1. Potential energy calculation

TPX09-v2 is a  $1/30^\circ \times 1/30^\circ$  global tidal atlas, based on a  $1/6^\circ \times 1/6^\circ$  global tidal solution merged with  $1/30^\circ \times 1/30^\circ$  local solutions for all coastal areas [19].<sup>1</sup> The M2 RMSE (Root-Mean-Square Error) for North Australia is 6.1 cm (compared to 10.2 cm for TPX09-v1), and 3.8 cm for North Australia Bays (compared to 5.1 cm for TPX09-v1). Twelve tidal constituents are available from TPX09-v2, five of which are used in this study (M2, S2, N2, K1 and O1) to capture both diurnal and semi-diurnal variability.

To calculate the theoretical tidal range resource, the potential energy (P.E.) of the tides is calculated at each  $1/30^\circ \times 1/30^\circ$  TPX09-v2 grid cell. Using T.TIDE, the tidal elevation time series for one year (2019) was predicted based on five tidal constituents, and the P.E. calculated over both flood and ebb phases of the tidal cycle:

$$\text{P.E.} = \sum_{i=1}^n \frac{1}{2} \rho g R_i^2 \quad (1)$$

where the subscript  $i$  denotes each successive rising and falling tide,  $\rho$  is the density of seawater,  $R$  is tidal range, and  $g$  is acceleration due to gravity. The P.E. density is calculated in units of  $\text{kWh}/\text{m}^2$ .

<sup>1</sup> Latest version available from <https://www.tpxo.net/global/tpxo9-atlas>.



## 2.2. Electricity generation via 0D modelling

In quantifying the energy that can be practically converted to electricity, the operation of tidal power plants must be simulated. The problem can be represented as distinct control volumes connected through hydraulic structures that regulate the transfer of water flows. In their simplest form, seaward water levels are prescribed and used as inputs to finite difference models as per the principles of mass conservation. In this study, 0D modelling methods [20,21] were applied.

A seaward water level time-series  $\eta_0(t)$  is used to calculate the head difference  $H$  that drives the flow between the sea and an impounded basin, or among connected basins. Continuity principles were then used to update the elevation of an impounded basin ( $\eta_1$ ). This type of modelling is referred to as 0D modelling and can be expressed in differential form as:

$$\frac{d\eta_1}{dt} = \frac{Q_3(m, H, t) + Q_4(m, H, t) + Q_{in}(t)}{A_b(\eta_1)} \quad (2)$$

where  $A_b$  is a function describing the wetted surface area of the tidal range structure (in  $m^2$ ) as per the impounded elevation  $\eta_1$ , and  $Q_3$  and  $Q_4$  represent the sluice gate and turbine flowrates, respectively, at any given point in time.  $Q_{in}$  (in  $m^3/s$ ) represents the sum of inflows/outflows through independent sources such as rivers or outfalls.

We consider single basin schemes where the elevation within the basin and the sea is sufficient for the model. An operational strategy is expected to update the elevation of an impounded basin ( $\eta_1$ ). This type of modelling is referred to as 0D modelling and can be expressed in differential form as:

The definitions of the flowrates  $Q_3$  and  $Q_4$  were determined through parameterizations based on the mode of operation  $m$  and head difference  $H$ . As the value of  $m$  is determined by the stage of the operation (Fig. 4), the flow through sluice gates typically has the following form [20]:

$$Q_3(m, H, t) = \begin{cases} r(t) \cdot \text{sgn}(H) \cdot C_d \cdot A_d \cdot \sqrt{2g|H|} & \text{for } m \in \{3, 4, 8, 9\} \\ 0 & \text{otherwise} \end{cases} \quad (3)$$

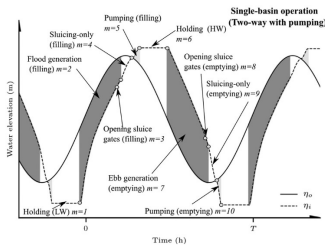


Fig. 4. Tidal power plant operation for a single basin scheme with two-way generation and pumping. Regions shaded in grey represent time periods when power is generated.

where  $A_d$  is the aggregated cross-sectional flow area (in  $m^2$ ) of the sluice gates, and  $\text{sgn}(\cdot)$  returns the sign ( $-1$  or  $1$ ) of a given quantity; in this case the head difference  $H$  to indicate the direction of the flow.  $C_d$  is the sluice gate discharge coefficient that is dependent on the design of the sluice gates [22], and  $r(t)$  is a ramp function representing the opening and closing of the hydraulic structures. The flow of turbines is parameterized based on a Hill Chart that represents the behaviour of the selected technology, as in Fig. 5. The individual turbine Hill Chart informs the tidal turbine flow rate  $Q_t$  ( $m^3/s$ ) and power output  $P_t$  (MW) [20], which can then be computed as:

$$Q_t(m, H, t) = \begin{cases} -r(t) \cdot \text{sgn}(H) \cdot N \cdot Q_b & \text{form } \in \{6, 10\} \\ r(t) \cdot \text{sgn}(H) \cdot N \cdot Q_{\text{chart}}(H) & \text{form } \in \{2, 3, 7, 8\} \\ r(t) \cdot \text{sgn}(H) \cdot N \cdot C_t \cdot \sqrt{2g|H|} \cdot \pi D^2 / 4 & \text{form } \in \{4, 9\} \\ 0 & \text{otherwise} \end{cases} \quad (4)$$

$$P_t(m, H, t) = \begin{cases} -r(t) \cdot \rho \cdot g \cdot Q_b \cdot |H| / \eta_p & \text{for } m \in \{6, 10\} \\ r(t) \cdot P_{\text{chart}}(H) & \text{for } m \in \{2, 3, 7, 8\} \\ 0 & \text{otherwise} \end{cases} \quad (5)$$

where  $N$  is the number of turbines installed,  $Q_b$  ( $m^3/s$ ) is the pumping flow rate,  $Q_{\text{chart}}$  ( $m^3/s$ ) is the flow rate according to the Hill Chart parameterization (Fig. 5), and  $D$  (m) the turbine diameter.  $C_t$  is a non-dimensional turbine discharge coefficient,  $P_{\text{chart}}$  (MW) is the power calculated from the Hill Chart and  $\eta_p$  is a pumping efficiency, which is a function of  $H$  [23]. Once fluxes through hydraulic structures are defined, Eq. (2) can be integrated to update the impounded water level  $\eta_1$ , whilst also calculating the power  $P$  generated from the turbines based on the discharge (Fig. 5). For conventional tidal power plant cases, Eq. (2) only needs to be integrated for one basin. For cases with multiple connected basins, i.e. linked-basin systems like the scheme considered previously in Doctor's Creek, Eq. (2) must be integrated for each of the basins, as described by Angeloudis et al. [21].

Limitations of 0D modelling emerge in neglecting any changes in hydrodynamics by the presence of large-scale infrastructure. This can be addressed through 2D or 3D hydrodynamic modelling once prospective projects are better defined [26,27]. However, given its simplicity and computational efficiency, 0D modelling is appropriate for preliminary assessments and optimization analyses of relatively small schemes [28,29]. In the absence of detailed information about specific schemes, we adopt the assumptions

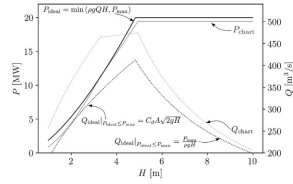


Fig. 5. Idealized and calculated tidal range double-regulated bulb turbine parameterization [24]. The Hill Chart Power ( $P_{\text{chart}}$ ) and discharge ( $Q_{\text{chart}}$ ) refer to the specifications listed in Table 1.  $P_{\text{max}}$  and  $A_t$  are the turbine capacity and the cross-sectional area, respectively. A detailed sequence to calculate the Hill Chart can be found in Aggidis and Feather [25].

discussed in Mejía-Olivares et al. [24] to determine a preliminary turbine and sluice gate configuration at sites of interest. The capacity  $C$  [W] was predicted as:

$$C = \eta \frac{\rho g \bar{A}_s \bar{H}^2}{T C_F}, \quad (6)$$

where  $\eta$  is the power plant efficiency,  $\bar{A}_s$  the mean surface area,  $\bar{H}$  the mean annual tidal range, and  $C_F$  is the capacity factor. The values of  $\eta = 0.55$  and  $C_F = 0.15$  are imposed in this analysis. The number of turbines was given as  $N_t = \frac{P_{max}}{P_{turb}}$ , where  $P_{max} = 20$  MW (Fig. 5). A number for the sluice gates ( $N_g$ ) must be estimated; here it is assumed that  $N_g = N_t/2$  with each individual gate having an effective cross-sectional area of 150 m<sup>2</sup>.

As the plant performance varies according to the power plant scheduling, a series of operational strategies were tested, with four parameters altered as introduced by Harcourt et al. [28]: holding duration over ebb ( $t_{he}$ ), holding duration over flood ( $t_{hf}$ ), pumping duration over ebb ( $t_{pe}$ ), pumping duration over flood ( $t_{pf}$ ). The specific values are summarized in Table 2. Ebb-only, Flood-only, Two-way and Two-way & pumping schedules impose fixed operation controls throughout the entire simulations. The remaining (Two-way [variable] and Two-way & pumping [variable]) strategies apply the optimization methods of Harcourt et al. [28] and Mackie et al. [29] to optimize the control values in every cycle, reflecting temporal tidal variations.

### 3. Tidal range resource

We first briefly present the theoretical global tidal range resource, before examining the theoretical and technical resource of Australia.

#### 3.1. Global tidal range resource

Initially, for comparison with previous studies, we calculate the theoretical global tidal range resource (Fig. 6). The global tidal range resource (excluding Hudson Bay due to extensive ice cover, consistent with previous studies) is 9115 TWh – an increase of 57% on the 5792 TWh estimated by Neill et al. [2] using the FES2014 dataset at a resolution of  $1/16^\circ \times 1/16^\circ$  (the resolution of TPX09-v2 used here is  $1/30^\circ \times 1/30^\circ$ ). This calculation is based on a minimum water depth of 30 m (i.e. to realistically and economically construct the embankment), and a minimum potential energy density of 50 kWh/m<sup>2</sup>.

Apart from the change in magnitude, Fig. 6 is qualitatively similar to previously published distributions of the tidal range resource, particularly Neill et al. [2], with the resource concentrated in a few shelf sea regions, including the northwest European shelf seas, Patagonian shelf, Bay of Fundy, and northwest Australia. As it has a substantial resource, and is the focus of this study, we examine the tidal range resource of Australia in the next section.

**Table 1**  
Turbine specifications associated with the Hill Chart presented in Fig. 5.

Capacity	$P_{max}$	20 MW
Turbine	$D$	7.35 m
Generator poles	$G_p$	95
Electricity grid frequency	$f_g$	50 Hz
Fluid density	$\rho$	kg/m <sup>3</sup>
Turbine discharge coefficient	$C_t$	1.36

#### 3.2. Australian tidal range resource

In this section, we examine the tidal range resource of Australia from both theoretical (Section 4.2.1) and technical (Section 4.2.2) perspectives.

##### 3.2.1. Theoretical resource

As expected from examination of the co-tidal charts (Fig. 3), the theoretical tidal range resource of Australia is concentrated in the Kimberley region of Western Australia, but other regions such as Broad Sound on the east coast of Queensland also contain a substantial resource (Fig. 7). Imposing a minimum water depth of 30 m (for the embankment) and a minimum annual energy density of 50 kWh/m<sup>2</sup> (for economics) the tidal range resource of Australia is 2004 TWh/yr (Fig. 8), or about 22% of the global resource. To put this in perspective, this exceeds Australia's total energy consumption for 2018/2019 (1721 TWh/yr),<sup>2</sup> suggesting tidal range energy has the potential to make a substantial contribution to Australia's electricity generation (265 TWh/yr in 2018/2019). Note that with the constraints of water depth and minimum threshold energy density, the Kimberley region is further highlighted as the principle tidal range hot spot of Australia (Fig. 8).

Although the resource distribution maps show the magnitude of the tidal range resource, they give no indication of temporal variability. To examine this, from a theoretical perspective, we investigated the phase diversity in the M2 tidal constituent (the dominant tidal constituent) over the Kimberley region (the discrete high energy region highlighted by Fig. 8). The phase difference over this region is  $10^\circ$  (over a length scale of order 1000 km), corresponding to a time difference of around 20 min, i.e. minimal phase diversity. However, there is an M2 amphidromic point just east of this region, close to Joseph Bonaparte Gulf (Fig. 3). This is also an amphidromic point for the other semi-diurnal constituents – S2 and N2. Examining the M2 phase of the large amplitude tides within the Joseph Bonaparte Gulf, there is potential for up to  $150^\circ$  phase difference between the Kimberley region and the Joseph Bonaparte Gulf. For this reason, a site in Kimberley (King Sound) is combined with a site in the Joseph Bonaparte Gulf for the technical resource assessment (Section 4.2.2), with consideration of aggregated power output between the two locations.

##### 3.2.2. Technical resource

0D modelling was applied at two sites that feature promising levels of potential energy, and complementary phase diversity. The focus here was on the two sites with the simulation results summarized in Table 3, including the normalized energy density, the overall plant efficiency ( $\eta$ ) that indicates the fraction of the potential energy extracted, and the capacity factor  $C_F$  of the turbine devices installed. As well as being characterized by a high tidal range, King Sound was selected as it has a history of tidal range project development [9,10]. Joseph Bonaparte Gulf was selected for the technical resource assessment as it has semi-diurnal tides that are around  $150^\circ$  out of phase, and hence are complementary with, King Sound. As the sites are around 600 km apart, there is some potential for phase diversity, should grid infrastructure be improved, if the electricity from both sites was aggregated into a unified grid. Of further interest, King Sound is classified as diurnal ( $F = 0.1$ ) whereas the tides in Joseph Bonaparte Gulf are mixed (mainly semi-diurnal,  $F = 0.3$ ).

Time series of tidal elevations and potential energy density over a 15 day period showed variabilities over spring-neap and diurnal time scales, with a strong diurnal component at Joseph Bonaparte

<sup>2</sup> energy.gov.au.

**Table 2**  
Operational values and limits for alternative operation strategies.

	Mode Duration (h)		Pumping modes	
	Holding modes			
	$t_{h,F}$ [h]	$t_{h,E}$ [h]	$t_{p,F}$ [h]	$t_{p,E}$ [h]
Ebb-only	4.0	0.0	0.0	0.0
Flood-only	0.0	4.0	0.0	0.0
Two-way	3.0	3.0	0.0	0.0
Two-way & pumping	2.5	2.5	0.5	0.5
Two-way [variable]	$\in [0.0, 4.0]$	$\in [0.0, 4.0]$	0.0	0.0
Two-way & pumping [variable]	$\in [0.0, 4.0]$	$\in [0.0, 4.0]$	$\in [0.0, 1.0]$	$\in [0.0, 1.0]$

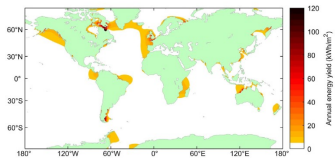


**Fig. 6.** Global tidal range resource, based on analysis of TPX09-v2, and without bathymetric constraints.

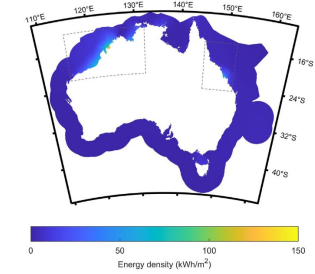


**Fig. 7.** Theoretical tidal range resource ( $\text{kWh}/\text{m}^2$ ) for all Australian EEZ (Exclusive Economic Zone). Bowed regions are shown in Fig. 8 with additional constraints on bathymetry and minimum energy density.

Gulf, and a very clear difference in phase between the two locations (Fig. 9). Implementation of various tidal range power plant operation strategies (flood-only, two-way, etc.) showed a range of power outputs and capacity factors (Table 4). The optimal solution for each location was achieved with two-way & pumping [variable], which achieved capacity factors of 18.1% (King Sound) and 16.6% (Joseph Bonaparte Gulf).

Considering time series of power output in more detail (Fig. 10),

the spring-neap cycle clearly maps onto the power output. With the larger tidal range at King Sound (mean 6.71 m compared to 5.35 m at Joseph Bonaparte Gulf, JBG – Table 3), peak power output is around  $34 \text{ MW}/\text{km}^2$  at King Sound during a spring tide – a 58% increase in peak power output compared to JBG (for a 25% increase in tidal range). With further optimization, it is possible to increase power output on the neap tides by around 96% (two-way & pumping [variable] compared to two-way & pumping) (Fig. 11). Although this leads to reduced variability over the fortnightly time scale, it is at the expense of considerable pumping, which would ideally be powered by other renewable sources. There is also strong asymmetry in the power signal at JBG compared to King Sound. Although we do not investigate the cause of this asymmetry in detail, it is likely due to the stronger diurnal signal at this location.

#### 4. Discussion

##### 4.1. Aggregated tidal power output

One of the challenges of tidal range power plants is the variability in power output associated with semi-diurnal tides. Although power output from a single tidal range power plant can be partially smoothed by optimization, e.g. two-way & pumping [variable] (Fig. 11), it is only through the development of multiple power plants that it may be possible to further smooth the (aggregated) power signal [e.g. 20]. This requires sites to be optimally selected based on the phase relationship of the semi-diurnal constituents – a scenario that has some potential in the Irish Sea, UK [30]. In Western Australia, we investigated two sites that display some complementary phase characteristics (King Sound and Joseph Bonaparte Gulf, JBG), because there is a  $150^\circ$  phase difference in the M2 constituent. Additional optimization in site selection could be achieved by applying optimization algorithms such as that presented by Neill et al. [30]. However, in the case of King Sound and JBG, the time series of power output for both sites is shown in Fig. 12. These time series demonstrate two key features relating to semi-diurnal and diurnal tides. Firstly, the semi-diurnal phasing between the two sites is clear, because there is only partial overlap of the power output. Ignoring capacity factor, each site generates electricity for around 34% of the time over a year. When aggregated, power is generated 45% of the time over a year – a considerable improvement in reducing the variability. Secondly, from Fig. 12, there is diurnal inequality in the power output at both locations. In King Sound this has the effect of alternating the magnitude of the power output between the flood and ebb operational phases of the tidal range power plant. However, for JBG, the signal is more complex and the power signal operates over a 48 h cycle. For example, and with reference to the bottom panel of Fig. 11, the tidal

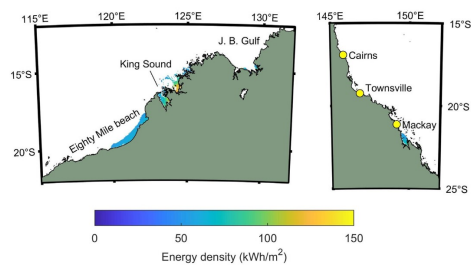


Fig. 8. Theoretical tidal range resource ( $\text{kWh}/\text{m}^2$ ) for Australian waters where depth  $< 30$  m and annual energy density exceeds  $50 \text{ kWh}/\text{m}^2$ . J. B. Gulf = Joseph Bonaparte Gulf.

**Table 3**  
Sites considered for tidal power plant operational models in Western Australia. The mean tidal range  $\bar{H}$  and available potential energy per area  $E_{\text{pot}}/A$  are based on the year 2019 at the selected sites.

Site	Latitude	Longitude	$\bar{H}_{2019}$ (m)	$E_{\text{pot}}/A$ ( $\text{GWh}/\text{km}^2$ )	$C/A$ ( $\text{MW}/\text{km}^2$ )
King Sound	16.89° S	123.65° E	6.71	103.2	37.2
Joseph Bonaparte Gulf	14.77° S	128.77° E	5.35	62.6	23.6

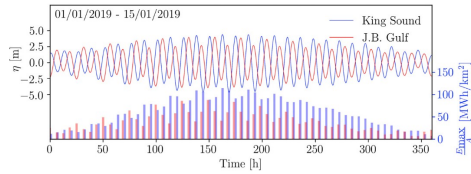


Fig. 9. Tidal elevations and area averaged potential energy for each tidal cycle at two selected sites: King Sound and Joseph Bonaparte Gulf (J.B. Gulf).

**Table 4**  
Summary of energy conversion predicted through 0D modelling for alternative operation strategies. All cases considered assumed the same turbine described by Fig. 5.

Name	Operation	$E/A$ ( $\text{GWh}/\text{km}^2$ )	$\eta$ (%)	$C_p$ (%)
King Sound	Ebb-only	31.34	30.37	9.63
	Flood-only	28.01	27.15	8.61
	Two-way	43.61	42.26	13.40
	Two-way & pumping	52.75	51.13	16.21
	Two-way [variable]	52.53	50.91	16.14
Joseph Bonaparte Gulf	Two-way & pumping [variable]	58.86	57.04	18.08
	Ebb-only	17.31	27.63	8.38
	Flood-only	15.89	25.37	7.70
	Two-way	25.30	40.38	12.25
	Two-way & pumping	29.24	46.66	14.16
	Two-way [variable]	27.69	44.19	13.41
	Two-way & pumping [variable]	34.30	54.75	16.61

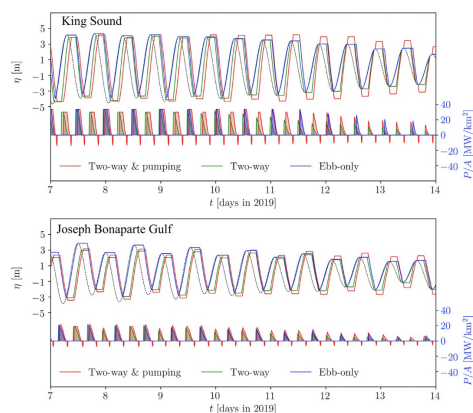


Fig. 10. Operation of tidal power plants over a transition from spring to neap tides, considering generic Ebb-only, Two-way and Two-way & pumping strategies. Note that negative power output indicates pumping.

range varies in the sequence 7.9 m (flood), 6.7 m (ebb), 5.4 m (flood), 6.5 m (ebb), 7.7 m (flood), etc. The result of this cycling through variations in tidal range every two days is a sequence of three larger (equal) tidal power outputs (regardless of flood or ebb) followed by a smaller power output on the next flood tide, and the sequence, although more apparent during spring tides, continues. You can also see that, in addition to complementary phasing of the semi-diurnal currents, the diurnal inequalities between these two selected sites are also complementary, i.e. when one location experiences a relatively low power output (once per day), the other location experiences its higher output at that time.

#### 4.2. Practical constraints to tidal power

Despite the remoteness of the area and competition from thermal power stations, the renewables sector in Western Australia could be developed due to the possibility of an export market. Proposals currently exist to export solar-generated power from Pilbara, Western Australia, to Java, Indonesia [16], potentially as part of a Pan-Asian Energy Infrastructure [31]. It is possible that future tidal energy sites in the case study region could be linked to such export systems.

The geology of the Kimberley region could pose problems for proposed tidal energy stations. For example, many of the estuaries in Collier Bay have soft, silty bases; and both Collier Bay and King Sound are characterized by high sedimentation rates. These inhospitable conditions would make engineering works costly, particularly the construction of the embankment, and ultimately make projects economically unviable [7]. Further, when operational, there could be a net transport of sediment into the lagoon,

and regular dredging and disposal of material may be required to maintain the volume of the lagoon basin [32].

Further environmental challenges facing proposed tidal range developments in the region are related to the North Kimberley marine park,<sup>3</sup> established in 2016. As Western Australia's largest marine park, and its important role in preserving the marine environment and attracting tourism, tidal range power schemes proposed for the region from the 1960s [e.g. 9], and receiving approvals subject to a series of environmental conditions as recently as 2013, could now struggle with consenting requirements.

#### 5. Conclusions

The tidal range resource of Australia is 2004 TWh/yr – around 22% of the global resource. The resource is primarily concentrated in the Kimberley region of Western Australia, which, as it is fairly remote, could lead to difficulties with grid integration, although it represents an export opportunity to southeast Asia. Consideration of the technical resource demonstrates that by optimizing the operation of two complementary sites in this region, variability can be reduced at both diurnal and semi-diurnal scales.

#### Declaration of competing interest

The authors declare that they have no known competing financial interests or personal relationships that could have appeared to influence the work reported in this paper.

<sup>3</sup> <https://parks.dpaw.wa.gov.au/connect/read/great-kimberley-marine-park>.

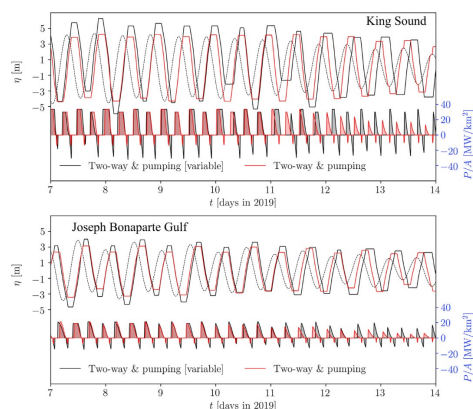


Fig. 11. Operation of tidal power plants over a transition from spring to neap tides, considering generic (in red) and optimized (in black) Two-way & pumping strategies. Note that negative power output indicates pumping.

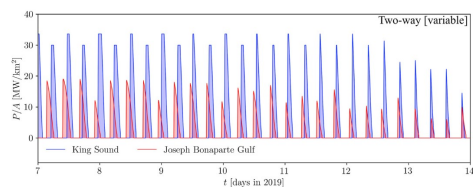


Fig. 12. Power output predicted for a Two-way (variable) operation at both selected sites: King Sound and Joseph Bonaparte Gulf.

### Acknowledgement

Simon Neill and Peter Robins acknowledge the support of SEEC (Smart Efficient Energy Centre) at Bangor University, part-funded by the European Regional Development Fund (ERDF), administered by the Welsh Government. Athanasios Angeloudis acknowledges the support of NERC through Industrial Innovation fellowship grant NE/R013209/2. We also thank two anonymous reviewers who provided useful comments on an earlier version of the manuscript.

### References

- [1] S.P. Neill, M.R. Hashemi, Fundamentals of Ocean Renewable Energy: Generating Electricity from the Sea, Academic Press, 2018.
- [2] S.P. Neill, A. Angeloudis, P.E. Robins, I. Walkington, S.L. Ward, I. Masters, M.J. Lewis, M. Plano, A. Aydis, M.D. Piggott, et al., Tidal range energy resource and optimization – past perspectives and future challenges, *Renew. Energy* 127 (2018) 763–778.
- [3] Australian Government Department of Industry, Science, Energy and Resources, Quarterly Update of Australia's National Greenhouse Gas Inventory: March 2020, 2020.
- [4] Clean Energy Council, Clean Energy Australia Report 2020, 2020.
- [5] R. Elliston, M. Diesendorf, I. MacGill, Simulations of scenarios with 100% renewable electricity in the Australian national electricity market, *Energy Pol.* 45 (2012) 606–613.
- [6] Australian Energy Market Operator, 2020 Integrated System Plan, 2020.
- [7] D. Harries, M. McInerney, P. Jennings, C. Thomas, Hydro, tidal and wave energy in Australia, *Int. J. Environ. Stud.* 63 (6) (2006) 803–814.
- [8] P. Marsh, I. Peneisis, J.R. Nader, R. Cossu, Multi-criteria evaluation of potential Australian tidal energy sites, *Renew. Energy* (2021) (in press).
- [9] J.G. Lewis, The Tidal Power Resources of the Kimberleys, Institution of Engineers, 1963.
- [10] Hydro Tasmania, Study of Tidal Energy Technologies for Derby, Sustainable

- Energy Development Office, Government of WA, 2001.
- [111] R.H. Charlier, Forty candles for the Rance River TPP tides provide renewable and sustainable power generation, *Renew. Sustain. Energy Rev.* 11 (9) (2007) 2032–2057.
- [112] C. Hendry, The role of tidal lagoons, Final Report (2016) p.95.
- [113] A.J. Clarke, D.S. Battisti, The effect of continental shelves on tides, *Deep Sea Research Part A, Oceanographic Research Papers* 28 (7) (1981) 665–682.
- [114] A. Iyer, S. Couch, G. Harrison, A. Wallace, Variability and phasing of tidal current energy around the United Kingdom, *Renew. Energy* 51 (2013) 343–357.
- [115] S.P. Neill, M.R. Hashemi, M.J. Lewis, Tidal energy leasing and tidal phasing, *Renew. Energy* 85 (2016) 580–587.
- [116] N. Ralph, L. Hancock, Energy security, transnational politics, and renewable electricity exports in Australia and Southeast Asia, *Energy Research & Social Science* 49 (2019) 233–240.
- [117] Sun Cable, Australia-ASEAN power link, <https://www.suncable.sg/> accessed: 03-11-2020.
- [118] The asian renewable energy hub, <https://asianrehub.com/> accessed: 03-11-2020.
- [119] G.D. Egbert, S.Y. Erofeeva, Efficient inverse modeling of barotropic ocean tides, *J. Atmos. Ocean. Technol.* 19 (2) (2002) 183–204.
- [120] A. Angeloudis, S.C. Kramer, A. Avdis, M.D. Piggott, Optimising tidal range power plant operation, *Appl. Energy* 212 (2018) 680–690.
- [121] A. Angeloudis, S.C. Kramer, N. Hawkins, M.D. Piggott, On the potential of linked-basin tidal power plants: an operational and coastal modelling assessment, *Renew. Energy* 155 (2020) 876–888.
- [122] A. Baker, Tidal power, *IEE Proceedings A Physical Science, Measurement and Instrumentation, Management and Education, Reviews* 134 (5) (1987) 392.
- [123] N. Yates, I. Walkington, R. Burrows, J. Wolf, The energy gains realisable through pumping for tidal range energy schemes, *Renew. Energy* 58 (2013) 79–84.
- [124] C.J. Mejia-Olivares, I.D. Haigh, A. Angeloudis, M.J. Lewis, S.P. Neill, Tidal Range Energy Resource Assessment of the Gulf of California, *Renewable Energy, Mexico*, 2020.
- [125] C. Aggidis, O. Feather, Tidal range turbines and generation on the Solway Firth, *Renew. Energy* 43 (2012) 9–17.
- [126] A. Angeloudis, R.A. Falconer, Sensitivity of tidal lagoon and barrage hydrodynamic impacts and energy outputs to operational characteristics, *Renew. Energy* 114 (A) (2017) 337–351.
- [127] A.L. Baker, R.M. Craghead, E.J. Jarvis, H.C. Stenton, A. Angeloudis, L. Mackie, A. Avdis, M.D. Piggott, J. Hill, Modelling the impact of tidal range energy on species communities, *Ocean Coast Manag.* 193 (2020) 105221.
- [128] J. Harcourt, A. Angeloudis, M.D. Piggott, Utilising the flexible generation potential of tidal range power plants to optimise economic value, *Appl. Energy* 237 (2019) 873–884.
- [129] L. Mackie, D. Coles, M. Piggott, A. Angeloudis, The potential for tidal range energy systems to provide continuous power: a UK case study, *J. Mar. Sci. Eng.* 8 (10) (2020).
- [130] S.P. Neill, M.R. Hashemi, M.J. Lewis, Optimal phasing of the European tidal stream resource using the greedy algorithm with penalty function, *Energy* 73 (2014) 997–1006.
- [131] S. Taggart, G. James, Z. Dong, C. Russell, The future of renewables linked by a transnational Asian grid, *Proc. IEEE* 100 (2) (2011) 348–359.
- [132] S.P. Neill, P.E. Robins, I. Fairley, The impact of marine renewable energy extraction on sediment dynamics, in: *Marine Renewable Energy*, Springer, 2017, pp. 279–304.